DOI 10.7343/as-2026-928

ACQUE SOTTERRANEE
Italian Journal of Groundwater

2026-AS56-928: 09 - 22

journal homepage: https://www.acquesotterranee.net/

An integrated geophysical and hydrogeological approach to aquifer vulnerability mapping: a case study from Ishielu, Ebonyi State

Integrazione di approcci geofisici e idrogeologici per la mappatura della vulnerabilità delle falde acquifere: il caso di studio a Ishielu, nello stato di Ebonyi

Johnson C. Ibuot [a], Stella J. Obidike[a], Daniel N. Obiora[a], Chidiebere O. Obasi[a]

a - Department of Physics and Astronomy, University of Nigeria, Nsukka.

ARTICLE INFO

Ricevuto/*Received*: 11 September 2025
Accettato/*Accepted*: 11 March 2026
Pubblicato online/*Published online*: 30 March 2026

Handling Editor:
Marco Pola

Editor in Chief:
Iacopo Borsi

Citation:
Ibuot, J.C., Obidike, J.S., Obiora, D.N., Obasi, O.C. (2026). An integrated geophysical and hydrogeological approach to aquifer vulnerability mapping: a case study from Ishielu, Ebonyi State.
Acque Sotterranee - *Italian Journal of Groundwater*, 15(1), 09 - 22
https://doi.org/10.7343/as-2026-928

Correspondence to:
Johnson C. Ibuot
johnson.ibuot@unn.edu.ng

Keywords:
Vertical Electrical Sounding, Aquifer Vulnerability Index, groundwater quality, physicochemical analyses, susceptibility.

Parole chiave:
sondaggi elettrici verticali, indice di vulnerabilità dell'acquifero, qualità delle acque sotterranee, analisi fisico-chimiche, suscettibilità.

Abstract

This study aims to appraise the vulnerability of aquifers in Ishielu Local Government Area, Ebonyi State, Nigeria, using an integrated approach that combines geoelectrical, hydraulic, and physicochemical analyses. The objective is to evaluate the extent of groundwater susceptibility to contamination and identify areas requiring protection. A total of 22 Vertical Electrical Soundings (VES) delineated four geoelectric layers, with dominating HA-type curves (28.6%). The third layer, identified as the aquifer unit, showed electrical resistivity values between 2.5 and 100.1 Ωm and thicknesses ranging from 14 to 121.1 m. Estimated hydraulic parameters indicated moderate porosity (28.5 - 32.5 %) and hydraulic conductivity (0.16 - 0.18 m/day), suggesting a moderate potential for contaminant transport. The Aquifer Vulnerability Index (AVI) was used to quantify the vulnerability of the subsurface and yielded Log C values between 1.04 and 1.89, classifying all sampled locations as highly vulnerable particularly in the northern and eastern zones. This is likely due to shallower water tables, thinner protective overburden, and more permeable lithologies in these areas. Hydrochemical analyses revealed elevated pH (8.9 - 9.9), high electrical conductivity (513 - 2,130 µS/cm), and iron concentrations (0.1223 - 0.9782 mg/L) exceeding WHO standards in several boreholes. Piper diagram interpretation identified the dominant water type as Ca - Cl, indicating both geogenic and anthropogenic influences on groundwater chemistry. The study suggests that aquifers in the area are highly vulnerable and recommends land-use control and continuous groundwater quality monitoring to safeguard public health.

Riassunto

Questo studio ha lo scopo di studiare la vulnerabilità degli acquiferi nell'area di governo locale di Ishielu, nello Stato di Ebonyi (Nigeria), utilizzando un approccio integrato che combina indagini geoelettriche, idrauliche e fisico-chimiche. L'obiettivo è quello di valutare il grado di suscettibilità delle acque sotterranee alla contaminazione e identificare le aree che richiedono protezione. Sono stati effettuati un totale di 22 sondaggi elettrici verticali (VES) che hanno evidenziato una predominanza di curve di tipo HA (28,6%). I risultati hanno permesso di individuare quattro orizzonti geoelettrici. Il terzo livello, identificato come l'acquifero, presenta valori di resistività compresi tra 2,5 e 100,1 Ωm e spessori variabili tra 14 e 121,1 m. I parametri idraulici stimati indicano una porosità moderata (28,5–32,5%) e una conducibilità idraulica compresa tra 0,16 e 0,18 m/giorno, suggerendo un potenziale trasporto di contaminanti moderato. L'Aquifer Vulnerability Index (AVI) è stato utilizzato per quantificare la vulnerabilità del sottosuolo evidenziando valori di Log C compresi tra 1,04 e 1,89 e classificando tutte le località campionate come altamente vulnerabili, in particolare nelle zone settentrionali ed orientali dell'area di studio. Questa caratteristica è probabilmente dovuta a livelli piezometrici più superficiali, ad una zona vadosa più sottile e a litologie più permeabili in queste aree. Le analisi idrochimiche hanno evidenziato valori elevati di pH (8,9 - 9,9), alta conducibilità elettrica (513 - 2.130 µS/cm) e concentrazioni di ferro (0,1223 - 0,9782 mg/L) che in diversi pozzi superano gli standard dell'OMS. L'interpretazione del diagramma di Piper ha identificato come la facies idrochimica dominante sia Ca–Cl, indicando sia influenze geogeniche sia antropogeniche sulla chimica delle acque sotterranee. Lo studio suggerisce che gli acquiferi dell'area sono altamente vulnerabili e raccomanda il controllo dell'uso del suolo e un monitoraggio continuo della qualità delle acque sotterranee per salvaguardare la salute pubblica.

Introduction

Groundwater has become an indispensable natural resource for drinking, irrigation, and industrial uses, particularly in regions where surface water is either scarce, seasonal, or polluted (Hagage et al., 2025). In sub-Saharan Africa, and Nigeria in particular, the reliability and relative quality of groundwater have positioned it as the backbone of water supply for rural and peri-urban communities (Edet & Okereke, 2001; Tijani, 2003). However, this vital resource is increasingly under threat due to rapid population growth, agricultural intensification, unregulated waste disposal, and land-use changes that compromise aquifer integrity. These threats necessitate comprehensive groundwater protection and monitoring strategies, especially in regions undergoing developmental pressures with limited infrastructure for water quality management.

Contaminated groundwater may be caused by a combination of geogenic and anthropogenic (human-induced) factors which contribute to the presence of high ions content in the groundwater (El-Aassar et al., 2023). This can have serious economic, social, and environmental impacts on the affected communities and ecosystems. The movement and concentration of contaminants in groundwater are shaped by various factors, including the pace and spread of pollutants, human activities such as land use, and geogenic elements such as soil and aquifer characteristics, and hydrological processes (Ali et al., 2005; Choudhary et al., 2024; Ifediegwu & Chibuike, 2021; Suthar et al., 2009; Woszczyk et al. 2018).

Geogenic contamination is driven by natural geological processes, such as the weathering and dissolution of aquifer minerals, which can release elements like arsenic, fluoride, iron, or manganese into groundwater over long timescales. In contrast, anthropogenic contamination results from human activities including agricultural runoff carrying nitrates and pesticides, industrial effluents containing heavy metals and hydrocarbons, and leachates from landfills or sewage systems. While geogenic sources are typically linked to the lithological and geochemical characteristics of the aquifer, anthropogenic sources are more closely tied to land-use patterns and environmental management practices, often producing localized and temporally variable impacts (Baloch et al., 2021; Ifediegwu, & Chibuike, 2021).

Aquifer vulnerability is a critical concept in groundwater resource protection and refers to the intrinsic and specific susceptibility of groundwater systems to contamination from surface or near-surface activities (Ibuot et al., 2025a; Vrba & Zaporozec, 1994). It is largely influenced by natural hydrogeological characteristics such as soil permeability, unsaturated zone thickness, depth to the water table, lithology, and recharge rates. Identifying areas with high aquifer vulnerability helps prioritize monitoring efforts and informs land-use planning to mitigate risks of groundwater degradation (Foster et al., 2002). Several approaches have been developed to assess aquifer vulnerability, including overlay index methods like DRASTIC and SINTACS, process-based simulation models, and empirical indices such as the Aquifer Vulnerability Index (AVI). The AVI method, developed by Van Stempvoort et al. (1992), evaluates vertical vulnerability based on the hydraulic properties and thickness of geologic units overlying the aquifer. It is particularly effective in regions where vertical contaminant migration is the dominant pathway and where geophysical data such as Vertical Electrical Sounding (VES) can provide valuable insight into subsurface layering and electrical resistivity distribution (Ibuot et al., 2025b; Nageswara Rao et al., 2018; Obiora & Ibuot, 2020; Okolie et al., 2015). The integration of geoelectrical methods in vulnerability mapping provides a non-invasive and cost-effective means of acquiring spatially distributed data on subsurface lithology and aquifer characteristics (Olayinka & Olorunfemi, 1992).

Yet, geophysical methods alone may not fully capture the dynamic interactions between aquifers and surface-derived contaminants. Hence, combining AVI with physicochemical analysis of groundwater offers a more robust and integrated approach. Physicochemical analysis of groundwater samples provides direct evidence of water quality, revealing the presence and concentration of contaminants (Akoto et al., 2008; Babiker et al., 2007; Ibuot et al., 2019a; Okoroh & Ibuot, 2022; Subba Rao et al., 2022; 2024; Yakubu et al., 2022). This dual approach both assesses the potential vulnerability of the aquifer system and also provides evidence of current contamination status, thereby bridging predictive vulnerability assessments with real-time water quality monitoring.

Studies in southeastern Nigeria have often relied solely on geophysical or hydrochemical techniques to assess groundwater conditions (Azi et al., 2020; Aleke et al., 2018; Anosike et al., 2019; Ibuot et al., 2019a; Ifediegwu & Chibuike, 2021; Obiora et al., 2016; Okolie et al., 2015). Numerous studies have assessed groundwater quality and contamination risks, employing strategies such as integrated hydrochemical–geophysical analysis, geospatial vulnerability mapping, and long-term monitoring to identify pollution sources and guide sustainable management (Baloch et al., 2025; Bon et al., 2020; Dilpazeer et al., 2023; Iqbal et al., 2023; Nageswara Rao et al., 2018; Saha et al., 2019; Subba Rao et al., 2024; Verma et al 2020).

This study applies an integrative hydrogeophysical and hydrochemical approach to comprehensively appraise aquifer vulnerability in Ishielu Local Government Area (L.G.A.) of Ebonyi State, southeastern Nigeria. The area, situated within the Lower Benue Trough, is underlain predominantly by sedimentary formations of the Asu River Group and the Eze-Aku Shale, which exhibit contrasting hydrogeological characteristics (Obaje, 2009). Increasing anthropogenic activities-such as open refuse dumping, subsistence farming, and artisanal mining-pose growing risks to groundwater quality, a critical resource for the local communities. In the study area, anthropogenic impacts on groundwater quality are largely linked to;

- unregulated agricultural practices, including the excessive use of fertilizers and pesticides, which contribute nitrates, chlorides, and other agrochemicals to recharge zones.

- poorly managed domestic wastewater disposal and pit latrines, which introduce pathogenic and chemical contaminants; and
- artisanal mining activities, which can release heavy metals and alter natural hydrochemistry.

This research presents a novel integration of geoelectrical (VES)-derived Aquifer Vulnerability Index (AVI) with detailed physicochemical analyses to simultaneously evaluate both the potential and current state of aquifer contamination. This dual assessment approach enables cross-validation between subsurface vulnerability indicators and actual water quality data, resulting in a more robust and holistic understanding of contamination risks.

Materials and methods

Ishielu Local Government Area (L.G.A.) is located in Ebonyi State, southeastern Nigeria (Fig. 1). Geographically, it lies between 6°18'N and 6°32'N, and longitudes 7°35'E and 7°51'E, covering an estimated land area of approximately 872 km^2. It shares boundaries with Ezza North and South LGAs to the west, Ikwo L.G.A. to the south, and Udenu and Isi-Uzo LGAs in neighbouring Enugu State to the north. The landscape is characterized by gently undulating terrain with isolated hills and low-lying ridges (Ifediegwu & Chibuike, 2021). Drainage is primarily influenced by seasonal streams and rivers, notably the Ebonyi River, which flows southeastward and eventually joins the Cross River system. Natural vegetation in the area includes secondary forest and derived savannah, although deforestation and urbanization have significantly altered the native land cover. The climate in Ishielu is humid tropical, featuring a distinct wet season from April to October and a dry season from November to March. Annual rainfall ranges between 1,500 and 2,000 millimeters, while average temperatures fluctuate between 25°C and 32°C throughout the year (Aghamelu et al., 2013). The region maintains high relative humidity, typically between 60% and 80%, which supports moderate to high rates of infiltration

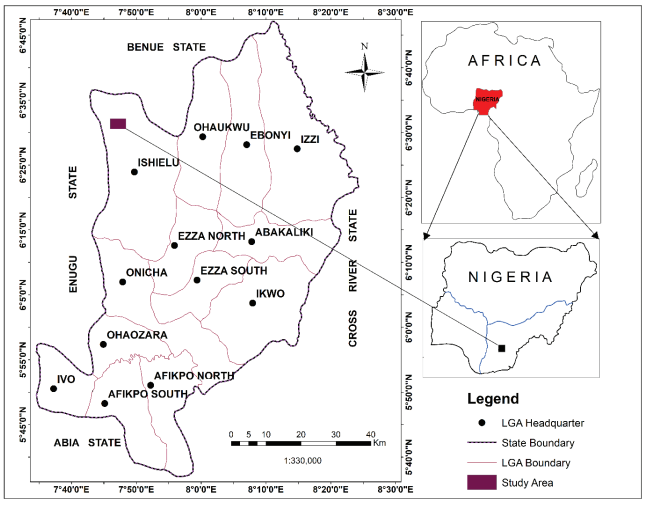

Fig. 1 - Map showing the location of Ishielu L. G. A.
Fig. 1 - Mappa che riporta l'area a governo locale di Ishielu.

and evapotranspiration. These climatic conditions play a vital role in groundwater recharge and water table fluctuations.

Geology and hydrogeology of the studied area

Geologically, Ishielu L.G.A. is part of the Lower Benue Trough (Obaje, 2009), a structural sedimentary basin that forms a component of the extensive West and Central African Rift System. The bedrock geology consists predominantly of sedimentary formations, notably the Asu River Group and the Ezeaku Formation (Reyment, 1965). The Asu River Group, which dates to the Albian stage of the Cretaceous, is composed of shale, siltstone, and fine-grained sandstones with occasional limestone lenses. This unit is generally low in primary porosity, though it can host groundwater in weathered or fractured zones. The Ezeaku Formation comprises the calcareous shales, fossiliferous sandstones, and interbedded limestone (Ofoegbu & Amajor, 1987; Obiora et al., 2016). This formation has more favorable conditions for groundwater occurrence due to the presence of coarser sediments and better-developed secondary porosity. The Awgu Formation is part of the upper Cretaceous sedimentary sequence, typically characterized by dark-grey to black shales and mudstones. It often contains thin limestone and sandstone interbeds, and is generally considered a potential source rock for hydrocarbons. In hydrogeological terms, it acts primarily as an aquitard or confining layer due to its low permeability. The Agala Formation consists mainly of sandstones, sandy shales, and occasional coal seams. The Agala Formation is more permeable and often functions as a minor aquifer where the sandstones are sufficiently thick and saturated. In the Ishielu area, weathered and fractured units within the Agala Formation can form shallow, local groundwater systems.

Hydrogeologically, the groundwater system in Ishielu is predominantly controlled by the degree of weathering and fracturing within the bedrock, as well as the thickness and permeability of the overburden layer. Two main aquifer types exist in the area. The first is a shallow, unconfined aquifer system occurring in the lateritic and weathered overburden, typically found at depths between 5 and 20 meters. This aquifer is directly recharged by rainfall infiltration and is highly vulnerable to contamination due to its shallow depth and lack of protective clay layers (Azi et al., 2020). The second is a deeper, semi-confined to confined aquifer found within fractured shale and sandstone bedrock units at depths ranging from 20 to 60 meters. Groundwater availability in these deeper aquifers is governed by the extent and connectivity of fractures and faults, which enhance permeability in otherwise low-porosity formations. This study focuses specifically on the vulnerability of the uppermost unconfined aquifer, as it is the primary source for local hand-dug wells and is most immediately exposed to surface contaminants. The deeper confined aquifer, while hydrologically significant, is not the subject of the vulnerability assessment presented here.

Groundwater flow within the region generally follows the natural topographic gradient, moving from elevated areas toward lower-lying zones and river valleys (Azi et al., 2020).

Recharge occurs mainly via direct infiltration of precipitation, with minimal contributions from surface water bodies due to limited hydraulic connectivity (Ofoegbu & Amajor, 1987).

Groundwater quality in the area is influenced by both natural geochemical conditions and anthropogenic activities. Preliminary hydrochemical assessments have reported elevated levels of iron, total dissolved solids (TDS), and nitrate in certain locations. These anomalies are often linked to leachate from open dumpsites, pit latrines, and runoff from agricultural lands where fertilizers and pesticides are widely used. Additionally, poor well construction and maintenance practices exacerbate the risk of aquifer contamination. The combined effects of geological structure, shallow water tables, and increasing land use pressure make it imperative to evaluate aquifer vulnerability in Ishielu L.G.A. through both geophysical and hydrochemical approaches.

Data collection

The methodology employed in this study integrates geophysical and physicochemical analyses to assess aquifer vulnerability across selected communities in Ishielu L.G.A.

Vertical Electrical Sounding (VES)

In this study, VES was employed to characterize subsurface geoelectric layers and delineate aquifer horizons, using the Schlumberger electrode configuration due to its high resolution, depth penetration, and efficiency in detecting subsurface hydrogeological variations, making it ideal for assessing aquifer characteristics and protective layers. This was done in twenty-two locations (Fig. 2) within the maximum current electrode spacing (AB) ranging from 1 to 900 m and potential electrode spacing (MN) ranging from 0.25 to 40 m. At each VES location, two current electrodes (A and B) were placed symmetrically about the survey centre and progressively expanded in equal increments to probe deeper subsurface layers, while two potential electrodes (M and N) remained near the centre to measure voltage differences. A direct current was introduced into the ground through the current electrodes, and the resulting potential difference was recorded alongside the injected current using the IGIS Resistivity meter model SSR-MP-ATS (https://www.igisindia.com). The apparent electrical resistivity (ρ_a) was calculated for each electrode spacing using the geometric factor (G) and the apparent resistance (R_a) expressed in equation 1. Measurements were repeated to minimize noise and ensure data reliability, with electrode positions adjusted to maintain optimal voltage response as the separation of current electrodes increased. The acquired ρ_a data were plotted against AB/2 on a log–log scale to generate sounding curves. To minimize noise and variability in the resistivity measurements, the resulting curves were smoothed, following methods described by Chakravarthi et al. (2007) and George et al. (2015), since the calculated apparent electrical resistivity values may contain random variations or measurement errors attributed to factors such as instrument noise, electrode contact issues, or natural variations in subsurface properties. Computer modelling was performed using the WinResist software (Vander Velpen, 2004) which iteratively adjusted theoretical models to fit measured data. The calculated apparent resistivity values served as input parameters and the software generated a series of geoelectric curves yielding estimates of layer resistivities, thicknesses, and depths within the subsurface layers investigated by the current penetration. The integration of VES with the Schlumberger electrode array enhanced delineating the subsurface electrical resistivity with depth (Lowrie, 1997; Telford et al., 1990).

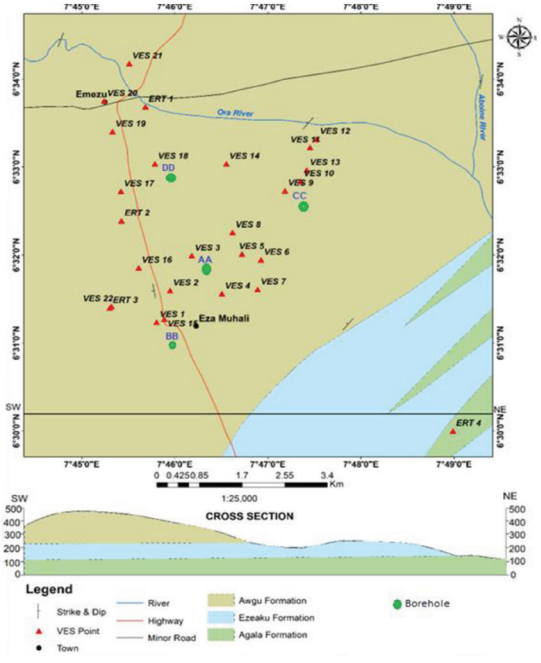

Fig. 2 - Map showing the geological setting of the study area and a cross section.

Fig. 2 - Carta che mostra l'assetto geologico dell'area di studio e una sezione geologica.

$$\rho_a = \pi \cdot \left[\frac{\left(\frac{AB}{2}\right)^2 - \left(\frac{MN}{2}\right)^2}{MN} \right] \cdot R_a \qquad (1)$$

where the geometric factor G is:

$$G = \pi \cdot \left[\frac{\left(\frac{AB}{2}\right)^2 - \left(\frac{MN}{2}\right)^2}{MN} \right] \qquad (2)$$

The contour maps were created to show the spatial trends of the geophysical parameters across the study area. Because the VES measurement points were irregularly spaced, we used the Kriging interpolation method in the Origin software (https://www.originlab.com). This method was chosen as it is best for estimating values at unsampled locations based on the spatial pattern of the existing data points.

Aquifer Vulnerability Index (AVI)

The AVI assesses the susceptibility of groundwater to pollution based on the thickness (h) and hydraulic conductivity

(K) of the vadose zone considered as the protective layers. AVI measures vulnerability through hydraulic resistance (C) to the vertical flow of water across the protective layers (Van Stempvoort et al., 1992) and was computed from h and K expressed in equation 3. The hydraulic resistance is a theoretical factor that explains the resistance of the aquifer protective layer to vertical flow.

$$C = \sum_{i=1}^{n} \frac{h_i}{K_i} \qquad (3)$$

Lower hydraulic resistance indicates that water and contaminants can more easily infiltrate into the aquifer, signifying higher vulnerability, while higher resistance suggests better protection and lower vulnerability. The values of K were determined using the Kozeny-Carman-Bear's equation expressed in equation 4 (Domenico & Schwartz 1990).

$$K = \left(\frac{\delta_w \cdot g}{\mu_d}\right) \cdot \left(\frac{d_m^{\,2}}{180}\right) \cdot \left(\frac{\phi^3}{(1-\phi)^2}\right) \qquad (4)$$

where g is the acceleration due to gravity (10 m/s²), δ_w is the density of water (1,000 kg/m³), d_m is the site's mean diameter (0.00036 m) measured using the micrometre screw gauge, and μd stands for the coefficient of dynamic viscosity of water, approximately 0.0014 kg/ms according to Fetters (1994).

The hydraulic conductivity (K) values obtained from equation 4 are uncertain regional estimates, not precise measurements. This is because porosity is indirectly estimated from electrical resistivity, and a uniform grain size is used for all layers. As a result, K is overestimated in fine materials and underestimated in coarse ones. Consequently, while these estimates provide valuable insight into relative permeability contrasts for regional aquifer characterization, they are not substitutes for locally measured hydraulic conductivities.

The effective porosity (ϕ) of the protective layers was calculated using equation 5 according to Ibuot et al. (2019b).

$$\phi = 36.51\rho^{-0.031} \qquad (5)$$

Where ρ is the electrical resistivity of the protective layers.

Table 1 outlines the correlation between hydraulic resistance (C) and the aquifer vulnerability index (AVI), assisting in the determination of vulnerability levels.

Tab. 1 - Relationship of aquifer vulnerability index (AVI) to hydraulic resistance (Van Stempvoort et al. 1992).

Tab. 1 - Correlazione fra le classi di aquifer vulnerability index (AVI) e la resistenza idraulica (Van Stempvoort et al., 1992).

Hydraulic resistance (C)	Log C	Vulnerability (AVI)
0 to 10	<1	Extremely high
10 to 100	1 to 2	High
100 to 1000	2 to 3	Moderate
1000 to 10,000	3 to 4	Low
>10,000	>4	Extremely low

Groundwater sampling and hydrochemical analysis

Groundwater samples were collected from four different boreholes (AA, BB, CC, and DD) in clean, acid-washed polyethylene bottles, and analyzed within recommended holding times. The water samples were divided into two containers: one for anions and the other for cations in order to determine their concentration in mg/L. A multi-parameter analyzer was used to measure pH and alkalinity. Alkalinity depends on the presence of certain chemicals such as carbonates, bicarbonates, and hydroxides (Thomas et al., 2020). The alkalinity was determined using the acid titration method. Water samples were titrated with a standardized sulfuric acid solution to the designated endpoint of pH 4.5, as indicated by the color change of an appropriate indicator (such as methyl orange or bromocresol green). The concentration of alkalinity was calculated based on the volume of acid consumed. The volume of acid used is then calculated to find the alkalinity concentration. The electrical conductivity of the water samples was measured at the collection point using a Wissenschaftlich-Technische Werkstätten LF91 meter, Model WTW LF 91 (Wissenschaftlich-Technische Werkstätten GmbH, Weilheim, Germany). Total dissolved solids (TDS) and dissolved oxygen (DO) were determined on-site. DO and TDS were measured with a dissolved oxygen meter and sensor. Chemical oxygen demand (COD) and biological oxygen demand (BOD) values were determined in the laboratory using standard procedures. The COD was measured by chemically oxidizing the water samples with dichromate under heat and measuring the oxygen consumed, while BOD was measured by incubating the samples for five days and calculating the oxygen depleted by microbial activity.

To ensure accurate analysis, the containers were initially cleaned with 0.05 M HCl and filtered through 0.45 μm pore membranes, then rinsed with deionized water. The water samples were acidified with concentrated nitric acid (HNO_3) to homogenize them and prevent metallic ions from adhering to the container walls. Cation concentrations (K^+, Na^{2+}, Ca^{2+}, Mg^{2+}, Mn^{2+}, and Fe^{2+}) were determined using the Atomic Absorption Spectrometer model AA-7000 Shimadzu, Japan ROM version 1.01 (https://www.shimadzu.com.au/products/elemental-analysis/atomic-absorption-spectroscopy/aa-7000/index.html), while anion concentrations (SO_4^{2-}, Cl^-, HCO_3^-) were determined in the laboratory using standard titrimetric methods. All procedures followed APHA (2017) standard methods to ensure accuracy, with results expressed in mg/L. The measured groundwater parameters were compared with WHO (2017) guidelines to evaluate potability. Stacked bar charts and piper diagram were used to summarize results.

To better interpret groundwater quality, the analyzed physicochemical parameters were presented using graphical tools. The stacked bar chart was used to illustrate the relative distribution of water quality parameters across sampling points. This visualization enables a clear comparison of parameter dominance, highlights spatial variability, and supports the identification of potential contamination trends. In addition, the Piper trilinear diagram was employed to

classify groundwater into distinct hydrochemical facies, revealing dominant cation - anion relationships and providing insights into geochemical evolution, mineral dissolution processes, and possible anthropogenic influences. Together, these tools enhance the interpretation of water chemistry results and their implications for aquifer vulnerability.

Results and discussion

VES

The interpreted electrical resistivity data obtained from twenty-two (22) VES points are summarized in Table 2. The variability in electrical resistivity, thickness, and depth across these points highlights the heterogeneous nature of the subsurface in the study area. Based on the VES interpretations, four distinct geoelectric layers were identified. Among the various types of curves observed, the HA-type was predominant, representing 28.6% of the total VES points. Other identified curve types included QH and QQ (each constituting 23.8%), HK (19.1%), and HQ (4.8%), as detailed in Table 2. In Vertical Electrical Sounding surveys, the curve types HA, QH, QQ, HK, and HQ are classifications used to describe four-layer subsurface electricl resistivity patterns. The letters derive from the standard three-layer types (H, K, A, Q), 'A' signifies a progressive increase in resistivity with depth, 'Q' signifies a progressive decrease, 'H' represents a low-resistivity intermediate layer, and 'K' represents a high-resistivity intermediate layer. Thus, a four-layer curve type like HA describes a sequence where the top three layers form an 'H' pattern (high-low-high), and the bottom three layers form an 'A' pattern (increasing electrical resistivity). Similarly, QH indicates a decreasing pattern followed by an 'H' pattern, QQ represents a continuous decrease in resistivity through all layers, HK signifies an 'H' pattern followed by a 'K' (high-resistivity intermediate) pattern, and HQ describes an 'H' pattern followed by a 'Q' (decreasing) pattern. These classifications help geophysicists interpret the geological structure and composition of the underground layers based on their electrical properties. The influence of the identified curve types on aquifer vulnerability is directly tied to their resistivity signatures, which reflect the protective capacity of overlying strata. The HA-type curves suggest moderate protective cover, while the presence of QH and QQ, HK, and HQ curve types indicates zones of reduced confinement and heterogeneous lithology, thereby highlighting areas of heightened aquifer vulnerability. The first (topmost) geoelectric layer exhibited electrical resistivity values ranging from 40.9 Ωm to 732.5 Ωm. Its thickness and depth varied between 0.4 m and 3.0 m. The second layer showed resistivity values between 2.2 Ωm and 73.4 Ωm. Thicknesses ranged from 1.2 m to 24.9 m, while depths extended from 3.7 m to

Tab. 2 - Summary of electrical resistivity survey in the study area.

Tab. 2 - Riepilogo delle indagini di resistività elettrica nell'area di studio.

VES No.	Long. (°E)	Lat. (°N)	Elevation (m)	Layer Electrical Resistivity (Ωm)				Layer thickness (m)			Layer depth (m)			Curve types
				ρ1	ρ2	ρ3	ρ4	h_1	h_2	h_3	d_1	d_2	d_3	
1	7.7634	6.5206	87	40.9	13	12	117.5	1.7	15	100.8	1.7	16.7	117.8	QH
2	7.7658	6.5266	87	208.7	10.5	100.1	10.3	1.2	2.5	14.0	1.2	3.7	17.7	HK
3	7.7697	6.5332	90	195.2	17.2	6.3	8.6	1.2	3.2	36.1	1.2	4.4	40.5	QH
4	7.7751	6.5260	80	120.8	15.4	12.3	87.1	1.2	8.2	103.1	1.2	9.4	112.5	QH
5	7.7787	6.5335	95	278.4	10.9	13.4	66.4	1.2	10.5	67.7	1.2	11.7	79.4	HA
6	7.7821	6.5324	84	77.3	8.9	10.4	19.6	1.3	6.7	115.2	1.3	7.9	123.2	HA
7	7.7815	6.5268	84	175.2	38.8	16.2	2.9	3	1.2	115.3	3	4.2	119.5	QQ
8	7.7770	6.5376	85	103.3	5.4	6.4	41.5	1.8	8.3	80	1.8	10.1	90.1	HA
9	7.7864	6.5455	93	375.3	28.6	34.1	3.7	1.3	17.7	91.1	1.3	19	110.1	HQ
10	7.7892	6.5473	99	732.5	8.2	46.6	19.7	0.9	19.1	61.9	0.9	19.9	81.8	HK
11	7.7909	6.5537	97	94.6	8.5	81.9	6.1	1.7	10.7	22.2	1.7	12.3	34.5	HK
12	7.7921	6.5553	100	205.5	12.9	15.8	16.7	1.3	24.9	69.5	1.3	26.2	95.7	HA
13	7.7903	6.5494	109	158.4	4.3	8.7	12.8	1.5	3.2	106.9	1.5	4.7	111.6	HA
14	7.7759	6.5506	95	135.3	73.4	2.5	14.8	0.8	4.2	20.5	0.8	4.9	25.5	QH
15	7.7648	6.5212	93	41.4	12.8	10.5	8.1	1.8	6.7	69	1.8	8.5	77.5	QQ
16	7.7602	6.5309	92	179.4	30.6	10.4	0.7	0.4	16.9	110.7	0.4	17.3	128	QQ
17	7.7570	6.5454	95	57.9	8.6	6.8	2.0	1.1	16.1	87.8	1.1	17.1	104.9	QQ
18	7.7631	6.5506	91	54.1	19.8	27.9	4.6	1.1	11.9	24.2	1.1	13	37.2	HK
19	7.7555	6.5567	104	268.8	24.1	8.7	0.6	1.1	10.3	121.1	1.1	11.4	132.5	QQ
20	7.7540	6.5625	91	131	2.2	3.8	97.9	1.5	11.3	30.2	1.5	12.8	43	HA
21	7.7585	6.5696	91	400.6	50.3	7.2	70.2	0.6	24.2	119.8	0.6	24.8	144.7	QH
22	7.7553	6.5236	100	216.3	8.0	27.8	167.4	1.6	6.1	27.2	1.6	7.7	34.9	HK

26.2 m. The third layer, identified as the saturated zone or aquifer, had resistivity values ranging from 2.5 Ωm to 100.1 Ωm. Thicknesses varied from 14.0 m to 121.1 m, and depths ranged between 17.7 m and 144.7 m. The fourth geoelectric layer exhibited resistivity values between 0.6 Ωm and 167.4 Ωm. However, its thickness and depth could not be precisely determined due to the limitations imposed by the maximum current electrode separation. The observed variations in electrical resistivity values reflect differences in lithology, moisture content, and pore-water chemistry, which have direct implications for aquifer vulnerability. The high-resistivity first layer offers limited protection if thin or fractured. This layer may be composed of dry lateritic soil, compacted sand, or rocky fragments. The low-resistivity second layer, which may be associated with clay-rich or silty deposits can act as a barrier but may permit contamination if permeable or discontinuous. The intermediate-resistivity third and fourth layers which may be dominated by sandy clay, weathered sandstone, or fractured bedrock, can store groundwater but are prone to pollution when protective layers are compromised, making the aquifer moderately to highly vulnerable.

Figure 3 demonstrates the comparison between VES curves (VES 3 and 15) and the lithological formations. The discrepancies between the borehole log and the electrical log may be due to conductive clays from the shale formations and variable saline groundwater which can make sandy layers appear as clay in VES data. Also, it is important to note that a perfect point-to-point match is not expected, as the VES method blends thin interbeds into broader units, while the borehole log shows detailed layering at a single point. Despite this scale difference, the agreement on major hydrogeological boundaries supports the validity of the geophysical interpretation for defining the aquifer architecture at a reconnaissance scale. These differences provide valuable insight into actual aquifer properties beyond simple lithology. Figures 4 and 5 shows the variation of electrical resistivity

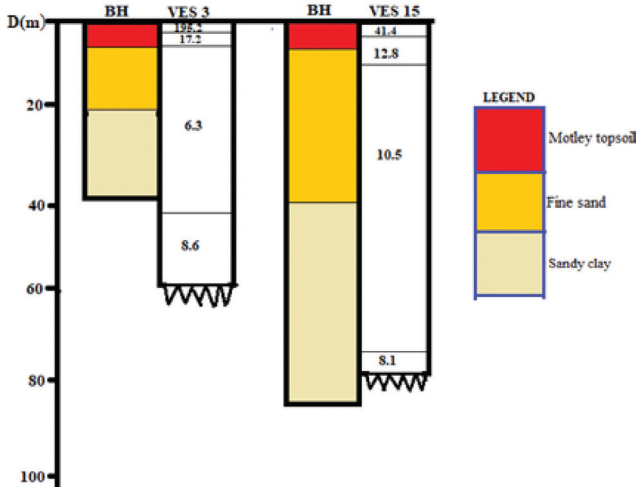

Fig. 3 - Comparison of vertical electrical sounding (VES) curves (VES 3 and 15) with the stratigraphic logs of nearby boreholes (BH). The numbers in the layers represent the electrical resistivity values in Ωm, D is depth in meters.

Fig. 3 - Confronto fra le curve ottenute mediante i sondaggi elettrici verticali VES 3 e 15 con le stratigrafie di pozzi limitrofi (BH). I numeri all'interno degli orizzonti rappresentano i valori di resistività elettrica in Ωm. D è la profondità in metri.

of the vadose zones (layer 1 and 2), where the highest resistivity values are observed in the eastern and northern parts respectively. The initial geoelectric parameters obtained from VES were utilized in equation 4 and 5 to determine the hydraulic conductivity and porosity of the vadose zones, while equation 3 was used in determining the hydraulic resistance (C) given in Table 3.

The porosity and hydraulic conductivity values of layers 1 and 2 (Table 3) reveal relatively consistent hydrogeological properties across the study area. Porosity in layer 1 (ϕ_1) ranges from 29.8% to 32.5% (mean = 31.2%, variance = 0.49), while in layer 2 (ϕ_2) varies between 28.5% and 31.7% (mean = 30.0 %, variance = 0.54), indicating a moderately porous unsaturated medium. Similarly, hydraulic conductivity

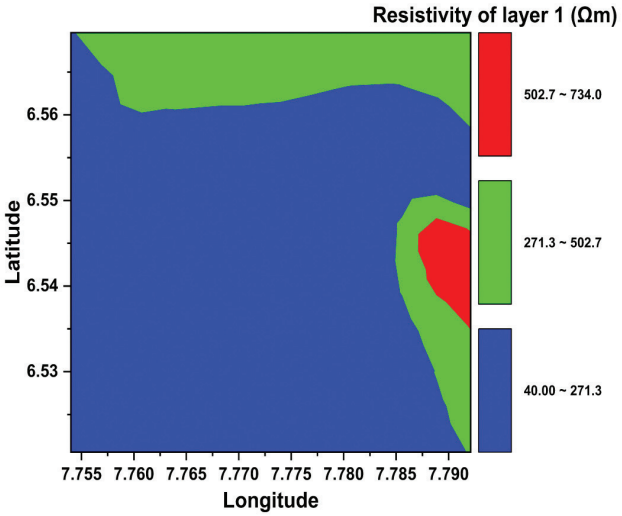

Fig. 4 - Variation of electrical resistivity of layer 1.

Fig. 4 - Variazioni di resistività elettrica nello strato 1.

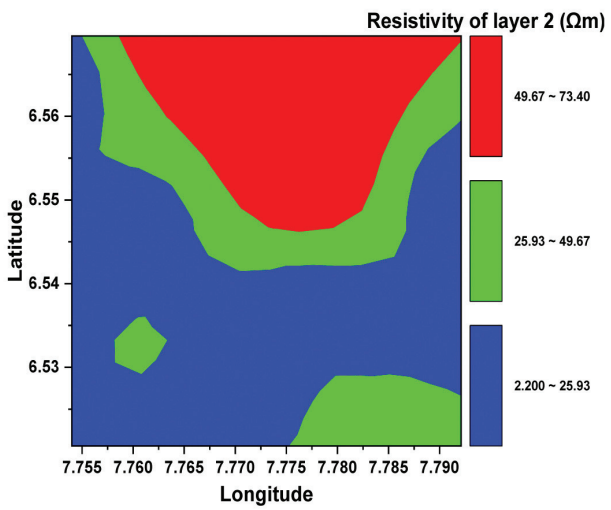

Fig. 5 - Variation of electrical resistivity of layer 2.

Fig. 5 - Variazioni di resistività elettrica nello strato 2.

in layer 1 (K_1) ranges from 0.16 to 0.18 m/day (mean = 0.17 m/day, variance = 1.46 × 10^{-5}), and in layer 2 (K_2) spans 0.16 to 0.17 m/day (mean = 0.17 m/day, variance = 1.42 × 10^{-5}), reflecting moderate permeability prone to contaminant transport. These values suggest that the vadose zone in the study area is relatively permeable, facilitating infiltration and vertical movement of water from the surface toward the saturated zone (Obiora & Ibuot, 2020). The minimal contrast in estimated porosity and hydraulic conductivity between lithologically distinct Layer 1 and Layer 2 is attributed to the homogenizing effects of pervasive weathering in the unsaturated zone. Although described differently in borehole logs, both layers consist of unconsolidated, fine-grained materials where weathering has produced a similarly porous and hydraulically resistive matrix. This result indicates that in this environment, the primary geologic origin of the materials is less influential on bulk hydraulic properties than the secondary weathering processes, leading to functional similarity despite lithological classification.

The hydraulic resistance (C), its logarithmic transformation (Log C), and the corresponding Aquifer Vulnerability Index (AVI) reveals critical insights into the groundwater protection status of the study area (Table 3). The C values calculated from equation 3 range from 11.0059 to 78.1455 days, with Log C values between 1.0416 and 1.8929. According to the rating of Van Stempvoort et al. (1992) in Table 1, Log C values below 2 signify high aquifer vulnerability. Notably, all 22 VES points fall within the "High" vulnerability category, indicating a widespread issue across the region. Since hydraulic resistance reflects the retardation offered by the overlying layer to the aquifer layer. The low resistance values observed here suggest that the protective cover is either thin or composed of permeable materials, allowing relatively rapid vertical migration of surface contaminants into the aquifer (Ossai et al., 2020; Ibuot et al., 2025). This means the aquifer is poorly protected and highly susceptible to pollution from agricultural runoff, industrial effluents, and domestic waste. The variation of C across the study area reveals highest values of C in the northern and eastern regions (Fig. 6), implying that these regions (with red colour in the contour map) are at considerable risk of groundwater contamination. As a result, there is a pressing need to enforce protective measures such as controlling land use practices, regulating waste disposal, and minimizing the use of agrochemicals near recharge zones. It also necessitates the implementation of best practices in borehole construction, such as proper casing and sealing, to prevent direct contamination pathways. Although the AVI method offers a useful baseline assessment, its dependence on limited hydrogeologic parameters may overlook subsurface complexities; incorporating additional techniques such as DRASTIC, numerical groundwater flow and transport simulations, or GIS-based multi-criteria approaches could

Tab. 3 - Summary of estimated hydrogeologic parameter.

Tab. 3 - Riepilogo dei parametri idrogeologici calcolati.

VES No.	Long. (°E)	Lat. (°N)	ϕ_1 (%)	ϕ_2 (%)	K_1 (m/day)	K_2 (m/day)	C (day^{-1})	Log C	AVI
1	7.7634	6.5206	32.5	30.0	0.18	0.17	48.6343	1.687	High
2	7.7658	6.5266	30.9	30.2	0.17	0.17	11.0059	1.042	High
3	7.7697	6.5332	31.0	29.8	0.17	0.16	13.1674	1.120	High
4	7.7751	6.5260	31.5	29.9	0.17	0.16	27.8878	1.445	High
5	7.7787	6.5335	30.7	30.2	0.17	0.17	34.9679	1.544	High
6	7.7821	6.5324	31.9	30.4	0.18	0.18	23.3962	1.369	High
7	7.7815	6.5268	31.1	29.0	0.17	0.16	12.6928	1.104	High
8	7.7770	6.5376	31.6	30.9	0.17	0.17	29.4544	1.469	High
9	7.7864	6.5455	30.4	29.3	0.17	0.16	57.8233	1.762	High
10	7.7892	6.5473	29.8	30.5	0.16	0.17	60.3644	1.781	High
11	7.7909	6.5537	31.7	30.4	0.17	0.17	36.3489	1.561	High
12	7.7921	6.5553	31.0	30.0	0.17	0.17	78.1453	1.893	High
13	7.7903	6.5494	31.2	31.1	0.17	0.17	13.7471	1.138	High
14	7.7759	6.5506	31.4	28.5	0.17	0.16	15.1852	1.181	High
15	7.7648	6.5212	32.5	30.0	0.18	0.17	24.7532	1.394	High
16	7.7602	6.5309	31.1	29.2	0.17	0.16	52.1278	1.717	High
17	7.7570	6.5454	32.2	30.4	0.18	0.17	50.0620	1.700	High
18	7.7631	6.5506	32.3	29.6	0.18	0.16	38.2415	1.583	High
19	7.7555	6.5567	30.7	29.5	0.17	0.16	34.4406	1.537	High
20	7.7540	6.5625	31.4	31.7	0.17	0.17	36.9752	1.568	High
21	7.7585	6.5696	30.3	28.8	0.17	0.16	76.1511	1.882	High
22	7.7553	6.5236	30.9	30.5	0.17	0.17	22.8272	1.359	High

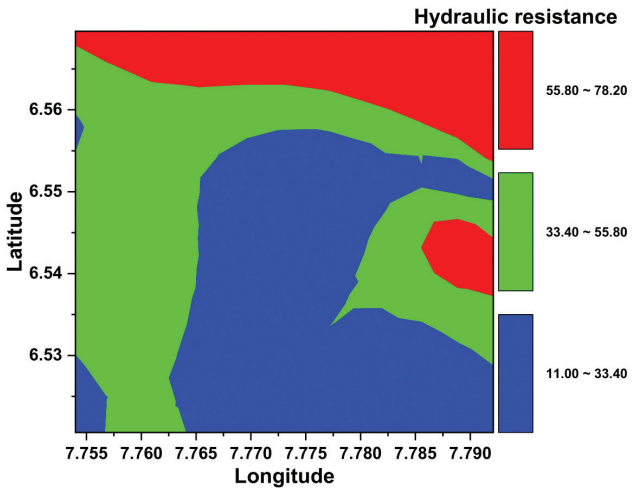

Fig. 6 - Contour map showing the variation of the calculated hydraulic resistance of the study area.

Fig. 6 - Carta delle variazioni di resistenza idraulica nell'area di studio.

improve accuracy and provide a more holistic evaluation of aquifer vulnerability.

A single-parameter removal analysis was performed to assess whether the overall mean Aquifer Vulnerability Index (AVI) was unduly influenced by any individual measurement. The result of the single-parameter removal analysis is presented in Table 4. The single-parameter analysis revealed that the mean Log C (1.54) is reasonably robust. The most influential points were the extreme values: the lowest hydraulic resistance point (C = 11.01 day^{-1}, Log C = 1.04) and the highest (C = 78.15 day^{-1}, Log C = 1.89). Removing these points changed the mean by approximately +1.7% and -1.1%, respectively. This indicates that while the overall spatial pattern is stable, the classification of the most extreme high- and low-vulnerability locations should be interpreted with caution, as they have a measurable effect on the statistical summary of the dataset.

Physicochemical characteristics of groundwater in the study area

Physicochemical parameters

The water quality analysis (Table 5) from four borehole samples (AA, BB, CC, and DD) highlights several critical water quality issues with implications for groundwater safety and public health. The results revealed the variations of the ions concentrations across the four boreholes considered in this study. The pH values, ranging from 8.9 to 9.9, exceed the WHO standard for drinking water (6.5–8.5) in all samples. The elevated pH values could be attributed to attributed to both geogenic and anthropogenic influences, which likely

Tab. 4 - Results of the Single Parameter Removal Analysis for the Aquifer Vulnerability Index (AVI).

Tab. 4 - Risultati dell'analisi di rimozione di un singolo parametro sull'indice AVI.

VES No.	Hydraulic Resistance, C (day^{-1})	Log C	Mean AVI with Point Removed	Change in Mean (Δ)	Influence on Mean (%)
1	48.6343	1.687	1.532	-0.008	-0.5%
2	11.0059	1.042	1.566	+0.026	+1.7%
3	13.1674	1.119	1.553	+0.013	+0.8%
4	27.8878	1.445	1.544	+0.004	+0.3%
5	34.9679	1.544	1.539	-0.001	-0.1%
6	23.3962	1.369	1.550	+0.010	+0.6%
7	12.6928	1.104	1.554	+0.014	+0.9%
8	29.4544	1.469	1.543	+0.003	+0.2%
9	57.8233	1.762	1.528	-0.012	-0.8%
10	60.3644	1.781	1.527	-0.013	-0.8%
11	36.3489	1.560	1.538	-0.002	-0.1%
12	78.1453	1.893	1.523	-0.017	-1.1%
13	13.7471	1.138	1.552	+0.012	+0.8%
14	15.1852	1.181	1.549	+0.009	+0.6%
15	24.7532	1.394	1.547	+0.007	+0.5%
16	52.1278	1.717	1.531	-0.009	-0.6%
17	50.0620	1.700	1.532	-0.008	-0.5%
18	38.2415	1.583	1.538	-0.002	-0.1%
19	34.4406	1.537	1.541	+0.001	+0.1%
20	36.9752	1.568	1.538	-0.002	-0.1%
21	76.1511	1.882	1.524	-0.016	-1.0%
22	22.8272	1.358	1.549	+0.009	+0.6%

result from the dissolution of carbonate-rich lithologies and feldspathic minerals, compounded by agricultural inputs such as lime-based amendments and fertilizers that enhance groundwater alkalinity and shift the groundwater chemistry toward basic conditions. Prolonged consumption of high-pH water can lead to gastrointestinal irritation and may also affect plumbing systems. The electrical conductivity (EC) values ranging from 513 to 2,130 µS/cm were also above WHO permissible limits of 1,500 µS/cm, indicating a high concentration of dissolved salts. This reflects slight to moderate salinity in the groundwater; the elevated electrical conductivity suggests potential salinity risks for agriculture and possible long-term health concerns from high dissolved salt. This highlights the dual need for monitoring suitability for both irrigation and drinking purposes, potentially making the water unpalatable and corrosive over time. Such EC levels are often associated with intensive land use, wastewater discharge, and natural mineral dissolution, aligning with previous studies by George et al. (2015b) and Akpan et al. (2015). Conversely, Total Dissolved Solids (TDS) levels, though variable (72.82–82.06 mg/L), remained within acceptable limits, signifying that while conductivity is high, the actual mass of dissolved solids is still relatively low. This may show ionic imbalances or the presence of specific conductive ions like chloride rather than large quantities of solids. Alkalinity values which range between 1.8 and 2.9 mg/L are below WHO standard of 200 mg/L, suggesting low buffering capacity, meaning the water has limited ability to resist sudden pH changes, especially in the presence of acidic contaminants. This can make the groundwater chemically unstable and sensitive to further pollution. Then, from the land use context we may conclude that the dominant hydrochemical signature is anthropogenic, primarily from agricultural fertilizers and sanitation, superimposed on the natural geogenic background from weathering of the local sedimentary formations.

Dissolved Oxygen (DO) concentrations ranged from 4.8 to 12.8 mg/L, indicating generally oxic conditions in samples AA, BB, and CC (DO > 5 mg/L), while sample DD reflects anoxic conditions, pointing to oxygen-deprived environments likely due to microbial activity or organic pollution (Thomas et al., 2020). Elevated Biological Oxygen Demand (BOD) values (8 to 16 mg/L) and Chemical Oxygen Demand (COD) values (26.4 to 53.6 mg/L) in all samples exceeded WHO standards, signifying a high load of biodegradable and chemical organic matter in the water. This poses serious concerns, as high BOD and COD levels can deplete oxygen in groundwater and promote anaerobic microbial processes, possibly leading to nitrate, sulfate, or heavy metal mobilization.

Hydrogeochemical parameters

The analysis of ionic concentrations (Table 4) in the groundwater samples reveals essential insights into the hydrogeochemical characteristics and water quality status of the study area. The anion distribution follows the order $Cl^- > SO_4^{2-} > HCO_3^-$, with HCO_3^- below detectable limit (BDL) in all samples. This absence of bicarbonate indicates a scarcity of carbonate-rich compounds and limited buffering capacity (Ibuot et al., 2017; Okoroh & Ibuot, 2022). The SO_4^{2-} levels ranged from 4.03 to 6.05 mg/L, and Cl^- ranged from 18.46 to 38.34 mg/L, both of which are well within WHO standards. Although non-threatening at these concentrations,

Tab. 5 - Physicochemical results of groundwater samples from boreholes.

Tab. 5 - Risultati dell'analisi fisico-chimiche sui campioni di acque sotterranee dei pozzi.

S/N	Parameters	AA	BB	CC	DD	WHO (2017)
1	pH	9.8	9.8	9.9	8.9	6.5 – 8.5
2	Electrical conductivity (µS/cm)	2,090	1,130	2,130	513	1,500
3	TDS (mg/L)	78.06	74.85	82.06	72.82	500
4	Alkalinity (mg/L)	2.8	2.6	2.9	1.8	200
5	DO (mg/L)	9.60	6.40	12.80	4.80	4
6	BOD (mg/L)	12.80	9.60	16.00	8.00	2
7	COD (mg/L)	42.40	32.00	53.60	26.40	10
8	SO_4^{2-} (mg/L)	4.99	4.03	6.05	4.80	250
9	Cl^- (mg/L)	32.66	19.88	38.34	18.46	250
10	HCO_3^-(mg/L)	BDL	BDL	BDL	BDL	200
11	Na^{2+} (mg/L)	8.39	8.08	8.05	7.83	200
12	K^+ (mg/L)	10.6	12.12	0.37	0.25	12
13	Ca^{2+} (mg/L)	16.00	73.33	78.67	13.33	75
14	Mg^{2+} (mg/L)	1.98	9.80	9.99	4.73	30
15	Mn^{2+} (mg/L)	0.03	0.26	0.10	0.10	0.5
16	Fe^{2+} (mg/L)	0.98	0.12	0.37	0.25	0.3
BDL: Below Detectable Limit						

the relatively elevated chloride levels suggest possible influence from surface contamination, agricultural runoff, or dissolution of chloride-bearing minerals. Continued rise in chloride levels could impact water palatability and signal early signs of contamination.

Cation concentrations followed the trend Ca^{2+} > K^{+} > Na^{+} > Mg^{2+} > Fe^{2+} > Mn^{2+}. Notably, Ca^{2+} ranged from 13.33 to 78.67 mg/L, and exceeded the WHO standard in samples BB and CC. This may be due to the presence of hard water, which though not a direct health threat, can cause scaling in pipes, boilers, and appliances, and may reduce the efficiency of soaps and detergents. Calcium's high presence also reflects interactions with carbonate rocks in the subsurface, consistent with groundwater traversing lithologies rich in calcareous materials. K^{+} and Na^{+}, with values ranging from 0.24 to 12.12 mg/L and 7.83 to 8.39 mg/L respectively, and remained within acceptable limits except K^{+} which exceeded WHO standard in sample BB. Though not problematic at current levels, they serve as indicators of geochemical alteration or anthropogenic input, particularly in agricultural areas. Mg^{2+} levels were also within safe limits, ranging from 1.98 to 9.99 mg/L, supporting the presence of moderate water hardness and confirming geogenic contributions from dolomitic or magnesian rocks.

However, the concentrations of Fe^{2+} ranged from 0.12 to 0.98 mg/L, exceeding the WHO limit (0.3 mg/L) in boreholes AA and CC. This can lead to aesthetic and operational issues such as staining, metallic taste, and biofouling. The elevated iron levels likely reflect geogenic inputs from Iron-bearing minerals (ferruginous sandstones and lateritic horizons) which under reducing conditions mobilize Fe^{2+} into groundwater (Ifediegwu & Chibuike, 2021), compounded by anthropogenic influences such as agricultural inputs, waste disposal, and borehole infrastructure corrosion. Mn^{2+} concentrations were within permissible limits (0.03 to 0.26 mg/L), though like iron, it is often naturally present due to rock weathering.

The physico-chemical characteristics indicate that the groundwater is being influenced by surface activities and may be vulnerable to progressive degradation. This aligns with earlier hydrogeological observations of high porosity and moderate permeability in the vadose zone, which allows rapid infiltration of surface water and pollutants into the aquifer. Therefore, the results call for urgent groundwater protection strategies, including land-use control, pollution source monitoring, and community awareness campaigns. Continuous water quality monitoring and remediation measures are also recommended to safeguard public health and ensure sustainable groundwater use in the region.

The Piper diagram (Fig. 7) provides insight into the hydrochemical characteristics of groundwater samples AA, BB, CC, and DD. When the cation and anion compositions are projected into the central diamond field, all the groundwater samples are classified as Ca-Cl water type. The predominance of the Ca-Cl water type, suggests a dual influence: geogenic contributions from carbonate and chloride-bearing formations, and anthropogenic inputs through agricultural activities and wastewater infiltration -together underscoring mixed contamination sources (Baloch et al., 2022). The Ca–Cl classification also implies that the groundwater is likely to be hard and may require treatment for domestic use. The clustering of the water samples in all three fields of the Piper diagram suggests a common hydrochemical origin or similar geological and environmental controls across the different sampling locations.

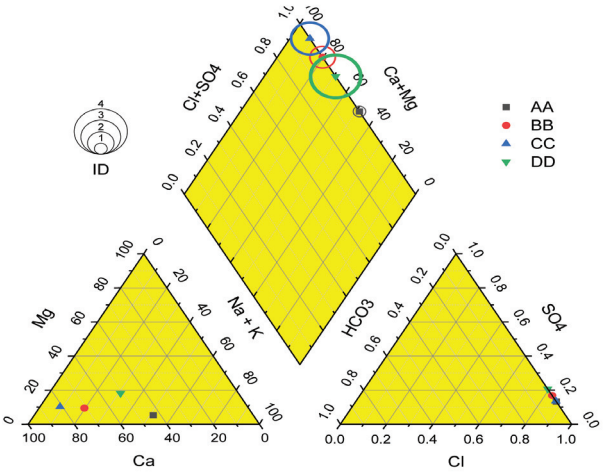

Fig. 7 - Piper trilinear diagram showing hydrogeochemical facies of groundwater.

Fig. 7 - Diagramma di Piper che mostra le facies idrochimiche delle acque sotterranee.

Conclusion

This study integrated geophysical and hydrochemical approaches to appraise aquifer vulnerability in Ishielu L.G.A. of Ebonyi State, Nigeria. The interpretation of VES data from 22 locations revealed a heterogeneous subsurface characterized by four distinct geoelectric layers. The predominance of HA, QH, and QQ curve types indicated variability in lithologic composition and aquifer properties across the region. The third geoelectric layer, identified as the aquifer, showed moderately low electrical resistivity values and considerable thickness, reflecting significant groundwater storage capacity. However, the overlying vadose zones (layers 1 and 2) exhibited relatively high porosity (28.46–32.54%) and moderate hydraulic conductivity (0.1572–0.1781 m/day), indicating a permeable subsurface that facilitates vertical infiltration of surface water and contaminants. AVI classification confirmed high aquifer vulnerability across all locations due to thin or permeable overburden. This implies that the protective cover above the aquifer is either thin or highly permeable, making the groundwater system particularly susceptible to contamination. The northern and eastern regions exhibited the highest vulnerability, emphasizing the need for targeted protection strategies in these zones.

Physicochemical analysis of groundwater samples corroborated the vulnerability assessment. The water was generally alkaline (pH 8.9–9.9), with high electrical conductivity (513–2,130 µS/cm), suggesting increased salinity due to surface inputs or geogenic sources. Dissolved

oxygen levels were sufficient in most samples, but elevated BOD and COD values across all samples indicated organic pollution, particularly in sample DD, which exhibited anoxic conditions. Most major ions were within WHO limits, except for calcium and iron, which exceeded permissible thresholds, indicating the presence of hard water and potential geogenic contamination, respectively. The absence of bicarbonate and low alkalinity further emphasized the poor buffering capacity of the groundwater. The Piper trilinear diagram classified all groundwater samples as Ca–Cl type, confirming a common hydrochemical facies dominated by calcium and chloride ions. This water type, often linked to mineral dissolution and anthropogenic impacts, underscores the progressive mineralization and potential pollution risk in the aquifer system. The clustering of all samples within these facies suggests uniform geochemical control and consistent influence of surface activities across the study area.

The integration of hydrogeophysical data and water quality analysis provides compelling evidence that the aquifer system in Ishielu L.G.A. is highly vulnerable to contamination. The study highlights the urgent need for sustainable groundwater management practices, including strict land-use regulation, control of agrochemical application, and proper borehole construction standards. Public awareness campaigns and continuous monitoring are essential to safeguard groundwater resources and ensure the long-term health and sustainability of water supply systems in the region. The study also advocates continuous monitoring alongside measures such as land-use zoning, controlled agrochemical use, stricter effluent regulation, protective buffer zones, and integration of groundwater protection into local development policies to safeguard aquifers and ensure sustainability. We recommend that future studies should collect layer-specific grain data for more precise modeling.

Acknowledgement
The authors are grateful to the Atmospheric and Solid Earth Geophysics research group of the University of Nigeria, Nsukka, for their encouragement during this research. We also, sincerely thank the editor and the reviewers for critically reviewing our paper which helped us to improve its quality.

Competing interest
The authors declare no competing interest.

AI use declaration statement
The authors used [Deepseek] during the writing process to improve readability and grammar in some parts of the paper. All AI-generated suggestions were verified for factual accuracy by the authors. The authors confirm that the AI tool is not listed as a co-author.

Author contributions
All authors contributed to the study conception, design, methodology, and wrote the manuscript. They read and approved the final manuscript.

Funding
The authors did not obtain any funding for this study.

Additional information
DOI: https://doi.org/10.7343/as-2026-982
Reprint and permission information are available writing to acquesotterranee@anipapozzi.it
Publisher's note Associazione Acque Sotterranee remains neutral with regard to jurisdictional claims in published maps and institutional affiliations.

REFERENCES

Akoto, O., Bruce, T. N., & Darko, G. (2008). Heavy metals pollution profiles in streams serving the Owabi reservoir. African Journal of Environmental Science and Technology, 2(11), 354–359.

Akpan, A. E., Ebong, D. E., Ekwok, S.E. (2015). Assessment of the state of soils, shallow sediments and groundwater salinity in Abi. Cross River State, Nigeria, doi.org/10.1007/s12665-015-4014-6

Ali, I., Gupta, V. K., & Aboul-Enein, H. Y. (2005). Metal ion speciation and capillary electrophoresis: application in the new millennium. Electrophoresis 26(21):3988–4002. https://doi.org/10.1002/elps.200500216.

Aleke, C. G., Ibuot, J. C. and Obiora, D. N. (2018). Application of electrical resistivity method in estimating geohydraulic properties of a sandy hydrolithofacies: A case study of Ajali Sandstone in Ninth Mile, Enugu State, Nigeria. Arabian Journal of Geosciences, 11(12): 1 - 13.

Anosike, S., Ibuot, J. C., Obiora, D. N. and Ugbor, D. O. (2019). Geophysical and physicochemical investigation of groundwater repositories in Njaba LGA of Imo State, eastern Nigeria. International Journal of Environmental Science and Technology, 16(12): 8129 - 8146.

APHA (American Public Health Association), AWWA (American Water Works Association), & WEF (Water Environment Federation). (2017). Standard Methods for the Examination of Water and Wastewater (23rd ed.). Washington, D.C.: American Public Health Association.

Azi, A. O. Onyebueke, D. E., Abbey, M. E., & Aluge, U. D. (2020). Assessment of Groundwater Potentials at Ishielu L. G. A. of Ebonyi State, Nigeria. Asian Journal of Geological Research 3(4): 45-53.

Babiker, I. S., Mohamed, M. A. A., Hiyama, T., & Kato, K. (2007). A GIS-based DRASTIC model for assessing aquifer vulnerability in Kakamigahara Heights, Gifu Prefecture, central Japan. Science of the Total Environment, 345(1–3), 127–140. https://doi.org/10.1016/j.scitotenv.2004.11.005

Baloch, M. Y. J, Zhang, W., Zhang, D., Al Shoumik, B. A., Iqbal, J., Li, S., Chai, J., Farooq, M. A., & Parkash, A. (2022). Evolution Mechanism of Arsenic Enrichment in Groundwater and Associated Health Risks in Southern Punjab, Pakistan. International Journal of Environmental Research and Public Health, 19(20), 13325. https://doi.org/10.3390/ijerph192013325

Baloch, M. Y. J., Zhang, W., Chai, J., Al Shoumik, B. A., Tariq, A., Iqbal, J., Talpur, S. A., Hussain, S., & Khan, Z. (2025). Groundwater contamination, fate, and transport of fluoride and nitrate in Western Jilin, China: Implications for water quality and health risks. Environmental Chemistry and Ecotoxicology. https://doi.org/10.1016/j.enceco.2025.04.010.

Baloch, M.Y.J.; Zhang,W.; Chai, J.; Li, S., Alqurashi, M.; Rehman, G.; Tariq, A.; Talpur, S.A.; Iqbal, J.; Munir, M.; et al. (2021). Shallow Groundwater Quality Assessment and Its Suitability Analysis for Drinking and Irrigation Purposes. Water, 13, 3361.

Bon, A.F., Sylvain, A.D., Lucian, A.B., Cyrille, N., Steven, C., & Arouna, M. N. (2020). Contribution of a model of geostatistical electrical conductivity in the assessment of the water pollution index of the Quaternary aquifer of the Lake Chad basin (Kousseri-Cameroon). Arabian J. Geosci. 13, 170. https:// doi.org/10.1007/s12517-020-5142-1.

Chakravarthi, V., Shankar, G. B. K., Muralidharan, D., Harinarayana, T., & Sundararajan, N. (2007). An integrated geophysical approach for imaging sub-basalt sedimentary basins: case study of Jam River basin, India. Geophysics 72(6): B141–B147

Choudhary, S., Subba Rao, N., Chaudhary, M., & Das, R. (2024). Assessing sources of groundwater quality and health risks using graphical, multivariate, and index techniques from a part of Rajasthan, India, Groundwater for Sustainable Development, 27, 101356, doi.org/10.1016/j.gsd.2024.101356

Dilpazeer, F., Munir, M., Baloch, M.Y.J., Shafiq, I., Iqbal, J., Saeed, M., Abbas, M.M., Shafique, S., Aziz, K.H.H., Mustafa, A., et al. (2023). A Comprehensive Review of the Latest Advancements in Controlling Arsenic Contaminants in Groundwater. Water, 15, 478. https://doi.org/10.3390/w15030478.

Domenico, P. A., & Schwartz, F. W. (1990). Physical and chemical hydrogeology (p. 324). Hoboken: Wiley Press.

Edet, A. E., & Okereke, C. S. (2001). A regional study of some hydrogeological parameters of the Cross River State, southern Nigeria. Journal of African Earth Sciences, 33(4), 595–605. https://doi.org/10.1016/S0899-5362(01)00094-6.

El-Aassar, A. H., Hagagg, K., Hussien, R., Oterkus, S., & Oterkus, E. (2023). Integration of groundwater vulnerability with contaminants transport modeling in unsaturated zone, case

study El-Sharqia, Egypt. Environmental Monitoring and Assessment, 195(6). https://doi.org/10.1007/s10661-023-11298-3.

Fetter CW (1994) Applied hydrogeology, 3rd edn. Macmillan College Publishing Company, New York

Foster, S. S. D., Hirata, R., & Andreo, B. (2002). The aquifer pollution vulnerability concept: Aid or impediment in promoting groundwater protection? Hydrogeology Journal, 10(1), 4–10. https://doi.org/10.1007/s10040-001-0173-5

George, Nyakno. J., Ibuot, J. C., & Obiora, D. N. (2015a). Geoelectrohydraulic parameters of shallow sandy aquifer in Itu, Akwa Ibom State (Nigeria) using geoelectrical and hydrogeological measurements. Journal of African Earth Sciences 110: 52 – 63.

George, N. J, Ibanga, J. I, & Ubom, A. I. (2015b) Geoelectrohydrogeological indices of evidence of ingress of saline water into freshwater in parts of coastal aquifers of IkotAbasi South Niger. J Afri Earth Sci 109:37–46.

Hagage, M., Hewaidy, A. G. A., & Abdulaziz, A. M. (2025). Groundwater quality assessment for drinking, irrigation, aquaculture, and industrial uses in the waterlogged northeastern Nile Delta, Egypt: a multivariate statistical approach and water quality indices. Modeling Earth Systems and Environment, 11(1), 59.

Ibuot, J. C., Okeke, F. N., George, N. J., & Obiora, D. N. (2017). Geophysical and physicochemical characterization of organic waste contamination of hydrolithofacies in the coastal dumpsite of Akwa Ibom State, Southern Nigeria. Water Science and Technology: Water Supply, 17(6): 1626 - 1637.

Ibuot, J. C., Ekpa, M. M. M., Obiora, D. N., Aka, M. U. & Omeje, E. T. (2025a). Appraisal of Groundwater Vulnerability to Pollution using pollution-based indices in Alluvial Aquifer of Niger-Delta Nigeria. Water Conservation Science and Engineering, 10, doi.org/10.1007/s41101-025-00361-4.

Ibuot, J. C., George, N. J., Okwesili, A. N. & Obiora, D. N. (2019b). Investigation of litho-textural characteristics of aquifer in Nkanu West Local Government Area of Enugu state, southeastern Nigeria. Journal of African Earth Sciences, 157(2019): 197 - 207.

Ibuot, J. C., Obiora, D. N., Igwe, E. I. & Ugwu, N. M. (2025b). Evaluation of groundwater vulnerability using index-based model approach within parts of Nsukka Sedimentary Basin, Nigeria. Solid Earth Sciences, 10, doi.org/10.1016/j.sesci.2025.100232.

Ibuot, J. C., Okeke, F. N., Obiora, D. N. & George, N. J. (2019a). Assessment of impact leachate on hydrogeological repositories in Uyo, Southern Nigeria. Journal of Environmental Engineering and Science, 14(2), 97–107.

Ifediegwu, S. I. & Chibuike, I. E. (2021). GIS based evaluation of shallow aquifer vulnerability to pollution using DRASTIC model: a case study on Abakaliki, southeastern, Nigeria. Arabian Journal of Geosciences (2021) 14:2534 https://doi.org/10.1007/s12517-021-08811-8.

Iqbal, J., Su, C., Wang, M., Abbas, H., Baloch, M. Y. J., Ghani, J., Ullah, Z., & Huq, M. E. (2023). Groundwater fluoride and nitrate contamination and associated human health risk assessment in South Punjab, Pakistan. Environmental Science and Pollution Research, 30(22), 1–20. https://doi.org/10.1007/s11356-023-25958-x.

Lowrie W (1997). Fundamentals of geophysics. Cambridge University Press, New York.

Nageswara Rao, P.V., Appa Rao, S. & Subba Rao, N. Delineation of groundwater prospective zones from a delta region of India, using geoelectrical and water quality approach. Environ Earth Sci 77, 616 (2018). https://doi.org/10.1007/s12665-018-7786-7.

Obaje, N. G. (2009). Geology and mineral resources of Nigeria. Springer Science & Business Media. https://doi.org/10.1007/978-3-540-92685-6

Obiora, D. N., & Ibuot, J. C. (2020). Geophysical assessment of aquifer vulnerability and management: A case study of University of Nigeria, Nsukka, Enugu State. Applied Water Science, 10, 29. https://doi.org/10.1007/s13201-019-1113-7.

Obiora, D. N., Ibuot, J. C., George, N. J. & Offiah, S. U. (2016). Delineation of groundwater saturation indicators and their distributions in the complex argillaceous geological units of Ezza north local government area of Ebonyi State, Nigeria. Current Science. 110(4): 701 - 708.

Ofoegbu, C. O. & Amajor, L. C. (1987). A geochemical comparison of the pyroclastic rocks from Abakaliki and Ezillo, southeastern Benue Trough. Journal of Mining and Geology 1987;23(1&2): 45-51.

Okolie, E. C., Egboka, B. C. E., & Nwankwo, L. I. (2015). Geo-electric evaluation of aquifer vulnerability and groundwater quality in Awka and environs, southeastern Nigeria. Arabian Journal of Geosciences, 8, 5693–5707. https://doi.org/10.1007/s12517-014-1627-z

Okoroh, D. O. & Ibuot, J. C (2022). Hydrogeochemical assessment of groundwater quality: a case study of Federal College of Education (Technical), Omoku, Rivers State. Water Practice and Technology, 17(7): 1458 – 1469.

Olayinka, A. I., & Olorunfemi, M. O. (1992). Determination of geoelectrical characteristics in Okene area and implications for borehole siting. Journal of Mining and Geology, 28(2), 403–412.

Ossai, M. N., Okeke, F. N., Obiora, D. N. & Ibuot, J. C. (2020). Vulnerability assessment of hydrogeologic units in parts of Enugu North, Southeastern Nigeria, using integrated electrical resistivity methods. Indian Journal of Science and Technology, 13(34): 3495 - 3509.

Reyment, R. A. (1965) Aspects of the Geology of Nigeria, Ibadan uni. Press, Ibadan Nigeria.

Saha, S., Selim Reza, A. H. M. & Roy, M. K. 2019 Hydrochemical evaluation of groundwater quality of the Tista foodplain, Rangpur, Bangladesh. Applied Water Science 9, 198. doi:10.1007/s13201-019-1085-7.

Subba Rao, N., Das, R., Sahoo, H.K., & Gugulothu, S. (2024). Hydrochemical characterization and water quality perspectives for groundwater management for urban development, Groundwater for Sustainable Development, 24, 101071, https://doi.org/10.1016/j.gsd.2023.101071

Subba Rao, N., Dinakar, A., & Sun, L. (2022). Estimation of groundwater pollution levels and specific ionic sources in the groundwater, using a comprehensive approach of geochemical ratios, pollution index of groundwater, unmix model and land use/land cover – A case study. Journal of Contaminant Hydrology, 248, doi.org/10.1016/j.jconhyd.2022.103990.

Suthar, S., Preeti, B., Sushma, S., Pravin, K. M., Arvind, K. N. & Nagraj, S. P. (2009). Nitrate contamination in groundwater of some rural areas of Rajasthan, India. Journal of Hazard Materials. https:// doi.org/10.1016/j. jhazmat.2009.05.111.

Telford WM Geldart LP Sherif RE 1990. Applied geophysics. Cambridge University Press, Cambridge.

Thomas, J. E., George, N. J., Ekanem, A. M. & Nsikak, E. E. (2020). Electrostratigraphy and hydrogeochemistry of hyporheic zone and water-bearing caches in the littoral shorefront of Akwa Ibom State University, Southern Nigeria. Environmental Monitoring and Assessment, 192:505. doi. org/10.1007/s10661-020-08436-6.

Tijani, M. N. (2003). Groundwater contamination in Nigeria: Problems and solutions. Hydrogeology Journal, 11(2), 156–165. https://doi.org/10.1007/s10040-002-0227-2

Van Stempvoort, D., Ewert, L., & Wassenaar, L. (1992). Aquifer Vulnerability Index (AVI): A GIS-compatible method for groundwater vulnerability mapping. Canadian Water Resources Journal, 18(1), 25–37. https://doi.org/10.4296/cwrj1801025

Vander Velpen, B. P. A. (2004). WinResist version 1.0. Resistivity sounding interpretation Software. M.Sc. Research Project, ITC Limited.

Verma, P., Singh, P. K., Sinha, R. R., & Tiwari, A. K. (2020). Assessment of groundwater quality status by using water quality index (WQI) and geographic information system (GIS) approaches: A case study of the Bokaro district, India. Applied Water Science, 10(27), 7. https:// doi. org/ 10. 1007/ s13201- 019- 1088-4

Vrba, J., & Zaporozec, A. (1994). Guidebook on mapping groundwater vulnerability. International Contributions to Hydrogeology, Vol. 16. International Association of Hydrogeologists.

WHO 2017 Drinking Water Standards, Monitoring and Reporting, vol. 1 of Recommendations, 2nd edn. WHO, Geneva, Switzerland.

Woszczyk M, Spychalski W, & Boluspaeva L (2018). Trace metal (Cd, Cu, Pb, Zn) fractionation in urban industrial soils of Ust-Kamenogorsk (Oskemen), Kazakhstan-implications for assessment of environmental quality. Environmental Monitoring and Assessment, 190:362–377.

Yakubu, J. A., Okwesili, N. A., Ibuot, J. C. & Obiora, D. N. (2022). Assessment of aquifer protective strength and groundwater quality within the University of Nigeria, Nsukka campus using geophysical and laboratory techniques. International Journal of Energy and Water Resources, doi.org/10.1007/s42108-022-00201-4.